Article type : Research Article

Enzyme Modification and Oxidative Crosslinking using Carboxylate-, Phenol-and Catechol-Conjugated 1,8-Naphthalimides

Stacey Sova and Lisa A. Kelly*

Department of Chemistry and Biochemistry, University of Maryland, Baltimore County, Baltimore, MD 21250

* Corresponding author email: lkelly@umbc.edu (Lisa A. Kelly)

ABSTRACT

The ground- and excited-state interactions of β-alanine, tyrosine and L-dopa substituted 1,8 naphthalimides (**NI-Ala**, **NI-Tyr** and **NI-Dopa**) with lysozyme and mushroom tyrosinase were evaluated to understand the mechanism of oxidative modification. Photooxidative crosslinking of lysozyme was observed for all three conjugates. The yield was significantly reduced for **NI-Tyr** and **NI-Dopa** due to intramolecular electron transfer to the excited singlet state of the 1,8-naphthalimide. Incubation of **NI-Tyr** and **NI-Dopa** with mushroom tyrosinase resulted in an increased fluorescence from the naphthalimide, suggesting that the phenol and catechol portion of the conjugates are oxidized by the enzyme. This results

This article has been accepted for publication and undergone full peer review but has not been through the copyediting, typesetting, pagination and proofreading process, which may lead to differences between this version and the Version of Record. Please cite this article as doi: 10.1111/php.13110

demonstrates that the compounds bind in the active site of mushroom tyrosinase. The catalytic activity of mushroom tyrosinase to oxidize both tyrosine (monophenolase) and L-dopa (diphenolase) was modified by **NI-Tyr** and **NI-Dopa**. Monophenolase activity was inhibited and the diphenolase activity was enhanced in the presence of these conjugates. Detailed Michaelis-Menten studies show that both V_{max} and K_m are modified, consistent with a mixed inhibition mechanism. Collectively, the results show that the compounds interact in the enzyme's active site, but also modify the distribution of the enzyme's oxidation states that are responsible for catalysis.

INTRODUCTION

Protein complex formation is a key step in biological function, including catalysis (1). The most widely used techniques to determine protein-protein interactions are co-immunoprecipitation or pull-down assays, western-blot analysis and crosslinking (2-4). Immunoprecipitation and western blot require strong protein-protein interactions and are not suitable for transient interactions governed by weak van der Waal and hydrophobic forces. The weakly-bound complexes simply dissociate when subjected to these assays, potentially losing many critical interactions.

Weakly-bound complexes are often studied using crosslinking methods, where closely-associated interactions are locked in place via an induced covalent bond (2). Chemical crosslinkers are highly reactive and work well for small protein complexes. Disuccinimidyl suberate is a non-cleavable and membrane-permeable crosslinker that contains an N-hydroxysuccinimide which will crosslink molecules with free primary amines (2). However, the compound is very reactive and, under certain conditions, induces

biologically irrelevant crosslinks (5). Since the chemistry requires modification of the amino acid side chains, the structure and function of the enzyme is necessarily altered (6).

Aside from static structural probes, the interaction dynamics play a key role in biological function (5). The study of these dynamics requires tools that can be activated "on demand," often on a time scale faster than mechanical mixing. An understanding of complexation dynamics is important to inhibit or activate specific processes that are linked to disease. Photooxidative crosslinkers provide an alternative to chemical methods. Light delivery, via pulsed excitation, is fast and, depending on the mechanism, the photophysical deactivation processes occur on the nanosecond to microsecond time scale. Finally, the photon energy is available to drive reactions that are otherwise thermally inaccessible.

The mechanisms and scope of photoinduced crosslinking to probe biomolecular interactions have been reviewed (7). Light activation of tris(2,2'-bipyridyl) ruthenium(II) complexes, in the presence of a sacrificial oxidant, initiate protein-protein crosslinks via the one-electron oxidation of the amino acid side chain (1),(5-6). This technique has been used to study amyloid formations over time that result in neurological disorders like Parkinson's disease (7-12). The method has also been applied to wound sealing in clinical applications to crosslink tissue after injury (13-15). The chemistry is regioselective towards the oxidizable tyrosine, tryptophan, cysteine and methionine residues (7). However, since it is a diffusional process, it lacks site-specificity (6-7). Other photosensitizers, including Rose Bengal, have been used to initiate protein crosslinks through a similar radical mechanism. Treatment of keratoconus in the eye involves crosslinking of collagen (15-16). However, the lack of site-specificity is problematic in that the chemistry doesn't distinguish between structurally related proteins, including collagens, and results in undesired side effects (17). Genetically altered amino acids have been used to impart specificity. However, this approach necessarily biases against crosslink formation in complexes with native sequence and structure (7),(18).

1,8-naphthalene imides comprise a diverse class of molecules that have been widely studied. Certain of these, including amonafide and mitonafide, entered clinical trials due to their strong anti-cancer activity (19). The compounds can also be activated with long-wavelength UV light. Their electronically excited states initiate a variety of photochemistry, including oxidation of certain nucleobases and amino acids (20-22). Photooxidative crosslinking of RNase and collagen has been demonstrated using 1,8-naphthalimides that are functionalized at the 4-position of the ring (23-25). In all of these studies, the oxidative crosslinking occurred without the need for a codissolved additive.

In this paper, we combine the known photooxidative crosslinking ability of 1,8-naphthalimides with a phenol or catechol derivative to site-specifically modify the enzyme mushroom tyrosinase. The structures of the compounds are shown in Figure 1. Changes in fluorescence intensity were used to demonstrate specific interactions of the conjugates with the mushroom tyrosinase active site. Modification of the enzyme's monophenolase and diphenolase catalytic properties to oxidize tyrosine or L-dopa substrates, respectively, was used to understand how the conjugates interact with the enzyme. Since the fluorescence intensities of **NI-Tyr** and **NI-Dopa** increase upon addition of the enzyme, the compounds serve as convenient "light up" sensors of association of the oxidative crosslinker with the enzyme. Finally, the approach offers a general strategy for conjugating substrate analogues with photoactive molecules to site-specifically modify an enzyme.

MATERIALS AND METHODS

Materials. 1,8-Naphthalic anhydride (97%) was purchased from Acros and recrystallized 3 times in DMF (Fisher Chemicals ACS grade). L-tyrosine (99%), L-alanine (98%), N-acetyl tyrosine (98%) and L-Dopa (98%) were purchased from Sigma Aldrich. Sodium dodecyl sulfate (SDS) (99%), ammonium persulfate (APS) (98%), tris(hydroxymethyl)aminomethane(Tris base) (99%), monosodium phosphate and sodium dihydrogen phosphate (98%) were purchased from Acros and used as received. Acrylamide 40% Stock solution (Acrylamide: Bis-Acrylamide, 19:1) was purchased from FisherBiotech. Tetramethylethylene diamine (TEMED) (99%) was purchased from Alfa Aesar. Coomassie Brilliant Blue R-250 (50g) was purchased from Bio-rad Laboratories. Low molecular weight calibration kit for electrophoresis was purchased from Amersham Pharmacia Biotech UK. Water was purified using a Biocel A10 Milli-Q system with 18.2 μΩ resistivity. Other materials and solvents were obtained from commercial sources.

Lyophilized lysozyme from chicken egg white (MW 14,300; >40,000units/mg) and mushroom tyrosinase (isolated from *Agaricus bisporus* (>1000units/mg)) were purchased from Sigma Aldrich and used as received. Protein stock solutions were prepared by dissolving the solid in 10 mM pH 7.0 phosphate buffer. The concentration of protein solution was determined from the 280-nm extinction coefficient of lysozyme (37,646 $M^{-1}cm^{-1}$) (26) and by molecular weight of mushroom tyrosinase (120,000 kdaltons) (27).

The syntheses of the N-substituted 1,8-naphthalimides (**NI**) were carried out using previously modified procedures, or modification thereof.

N-(2-Ethanoic Acid)-1,8-Naphthalene Imide (NI-Ala). (28) UV (10 mM phosphate buffer pH 7.0) λ_{max} (ε): 344 nm (14600 ± 100 $M^{-1}cm^{-1}$), 234 nm (42200 ± 300 $M^{-1}cm^{-1}$), 214 nm (23000

± 400 $M^{-1}cm^{-1}$). ^{1}H NMR (DMSO-d_6): δ 8.53 (dd, 4H, naphth), 7.91 (t, 2H, naphth), 4.23 (d, 2H, CH_2), 2.61 (t, 2H, CH_2).

N-2-(4-Hydroxyphenyl)-1-carboxyethyl -1,8-Naphthalene Imide (NI-Tyr). (21)

UV (10 mM phosphate buffer pH 7.0) λ_{max} (ε): 344 nm (12600 ± 200 $M^{-1}cm^{-1}$), 274 nm (4200 ± 100 $M^{-1}cm^{-1}$), 234 nm (27300 ± 400 $M^{-1}cm^{-1}$). ^{1}H NMR (DMSO-d_6): δ 8.53 (dd, 4H, naphth), 7.92 (t, 2H, naphth), 6.83 (d, 2H, phen), 6.44 (d, 2H, phen), 5.78 (t, H, CH), 2.42 (m, 2H, CH_2).

N-(3,4-Dihydroxyphenyl)-1-carboxyethyl-1,8-Naphthalene Imide (NI-Dopa). 0.50 g L-dopa (0.0025 mol) and 0.48 g 1,8-naphthalic anhydride (0.0025 mol) were suspended in 30 mL DMF and the solution was heated to 120^{o}C for 3 hours. A viscous residue was obtained by rotary evaporation of the solvent under vacuum. The residue was treated with 15 mL deionized water to obtain 0.40 g crude solid. The precipitate was filtered and recrystallized 3 times in a 60% (v/v) solution of water and methanol, producing a pale brown powder. UV (10 mM phosphate buffer pH 7.0) λ_{max} (ε): 344 nm (12200 ± 100 $M^{-1}cm^{-1}$), 280 nm (3700 ± 100 $M^{-1}cm^{-1}$), 234 nm (32300 ± 200 $M^{-1}cm^{-1}$), 214 nm (23000 ± 300 $M^{-1}cm^{-1}$). ^{1}H NMR (DMSO-d_6): 8.41 (dd, 4H, naphth), 7.82 (t, 2H, naphth), 6.47 (d, H, phen), 6.34 (d, 2H, phen), 6.27 (dd, H, phenyl), 5.75 (dd, H, CH), 3.29 (dd, H, CH_2), 3.17 (m, H, CH_2). ^{13}C NMR (DMSO-d_6): 171.4, 163.5, 145.3, 144.0, 135.3, 131.8, 129.1, 127.9, 127.7, 121.9, 120.1, 116.8, 115.8, 54.7, 34.1 HRMS expected: 378.09721 amu; Found: 378.098010 amu.

Methods. Ground state UV-Vis absorption spectra were measured using a JASCO V-570 double beam spectrophotometer. An Edinburgh Instruments FLS920 spectrofluorimeter equipped with a 450 W Xenon lamp and Hamamatsu 5509-42 PMT (cooled to -80 ^{O}C) was used to acquire steady-state emission spectra. Fluorescence quantum yields were determined with optically matched solutions (344 nm) of the **NI**'s in a 10 mM pH 7.0 phosphate buffer. **NI-Ala** was used as a standard (Φ_f= 0.34) (21).

Photolyses. Steady state photolyses were carried out using a 450W mercury vapor-lamp (Ace Glass, Vineland, NJ). The samples were placed in 10-mL Pyrex tubes, maintained at 25^{o}C, and photolyzed in a turntable reactor. Filters (Schott WG320) were placed between the lamp and samples to prevent direct irradiation of the protein. Samples of each naphthalimide (OD 344-nm = 0.6) were co-dissolved with 80 μM lysozyme in 10 mM pH 7.0 phosphate buffer. Aliquots were removed every 30 minutes and diluted by a factor of 2 with loading buffer. Samples were run on an 18% SDS-PAGE gel, stained with Coomassie blue and then imaged.

Competition kinetics. The kinetics of monophenolase and diphenolase activites of mushroom tyrosinase were measured using substrates L-tyrosine and L-Dopa respectively. Substrate concentrations up to 1 mM were incubated with each naphthalene imide in 10 mM pH 7.0 phosphate buffer for 1 minute, followed by the addition of 43.3μg/mL mushroom tyrosinase (for monophenolase activity) or 4.33 μg/mL (for diphenolase activity) (29-31). After mixing, the reaction rates were determined by measuring the dopachrome formation at 475 nm over the course of 2-5 minutes (29),(32-34). Samples were maintained at 25^{o} C during the course of the reaction .

The oxidation reaction by mushroom tyrosinase followed Michaelis-Menten kinetics (eq 1) in the absence of naphthalimide.

$$V_o = \frac{V_{max}[S]}{K_m + [S]} \quad (1)$$

In eq 1, V_0 is the initial velocity, V_{max} is the maximum velocity of the reaction at saturating substrate conditions, S is substrate concentration and K_m, the Michaelis constant, is the substrate concentration where the rate of reaction is half that of V_{max}. The data were fit to the model using a nonlinear least squares regression to determine K_m and V_{max} at different naphthalimide concentrations.

RESULTS

Ground-State Absorption and Singlet-State Properties

The UV absorption and normalized fluorescence spectra of **NI-Ala**, **NI-Tyr** and **NI-Dopa** are shown in Figures 2 and 3, respectively. The spectral shapes of the 3 compounds are identical. However, the fluorescence intensities of **NI-Tyr** and **NI-Dopa** are more than 100 times smaller than that of **NI-Ala** (ϕ_f=0.34 ± 0.02) (21). The fluorescence quantum yields were found to be 0.0059 ± 0.0014 and 0.0027 ± 0.0012 for **NI-Tyr** and **NI-Dopa**, respectively.

Singlet-State Reactivity with Amino Acids and Proteins

Steady-state fluorescence measurements were used to determine the singlet excited-state reactivity of **NI-Ala** with tyrosine, L-dopa and lysozyme. The fluorescence of **NI-Ala** was quenched by the addition of L-dopa, as seen in Figure 4. Quenching was also observed with tyrosine and lysozyme with no shift in the fluorescence spectra. The fluorescence quenching data were fitted to a Stern-Volmer bimolecular quenching equation, eq 2 (35).

$$\frac{I_0}{I} = 1 + k_q \tau_f [Q] \qquad (2)$$

where I_0 and I are the fluorescence intensities without and with quencher Q (tyrosine, L-dopa and lysozyme), k_q is the bimolecular quenching constant and τ_f is the lifetime of ^{1}**NI-Ala***, determined from time-correlated single photon counting to be 2.1 ns. A linear Stern-Volmer plot was obtained for all quenchers. The Stern-Volmer plot for L-dopa is shown in the inset of Figure 4. The bimolecular quenching constants, k_q, for tyrosine, L-dopa and lysozyme, determined from the slope of the Stern-Volmer plot and the singlet state lifetime, are shown in Table 1. Bimolecular quenching constants for **NI-Tyr** and **NI-Dopa** were not determined because quenching was not observed at the quencher concentrations that were used.

Non-Specific Crosslinking

Steady-state photolyses of codissolved **NI**s and lysozyme were carried out to assess the non-specific interactions between each naphthalimide and the enzyme. No evidence of ground-state complexation was observed by UV spectroscopy. Samples of **NI-Ala**, **NI-Tyr** and **NI-Dopa** (80 μM) were codissolved with 50 μM lysozyme in pH 7.0 phosphate buffer. The samples were kept in the dark or simultaneously irradiated at 25^{o}C in a turntable reactor for 30 minutes. The samples were removed from irradiation and diluted by half with running

buffer. The photoproducts were then separated on an SDS-PAGE gel and visualized by a Coomassie Blue stain. The results are shown in Figure 5. Shown in lane 1 is the ladder of MW markers. Lysozyme, irradiated in the absence of **NI**s (Lane 2), is not modified by direct irradiation. When **NI-Ala** is irradiated for 30 minutes in the presence of lysozyme, bands at 28 kDa and 42 kDa are observed, consistent with formation of a lysozyme dimer and trimer (Lane 6). Faint molecular weight bands appear at 28 kDa when **NI-Tyr** (Lane 7) and **NI-Dopa** (Lane 8) are irradiated in the presence of lysozyme.

Site-specific enzyme targeting

Having demonstrated photoinduced crosslinking using the 1,8-naphthalimides, it was of interest to target specific binding sites of an enzyme. Mushroom tyrosinase enzymatically oxidizes both tyrosine and L-dihydroxyphenylalanine (L-Dopa) to their corresponding quinones (36). The naphthalimide conjugates containing these substrate analogs (**NI-Tyr** and **NI-Dopa**) were incubated (dark) with mushroom tyrosinase in 10 mM pH 7.0 phosphate buffer. Enzymatic modification of the conjugates was assessed using fluorescence spectroscopy. As seen from Figure 6, there is ca. 5-fold increase in fluorescence intensity after 2 hours of incubation. When the same experiment was carried out using **NI-Ala**, the fluorescence was unchanged. These results clearly show that the naphthalimide conjugates are enzymatically modified by mushroom tyrosinase.

Competitive enzyme kinetic assays were carried out to understand the nature of interaction between these naphthalene imides and mushroom tyrosinase. A solution of

naphthalene imide was mixed with varying concentrations (0-1 mM) of either tyrosine or L-dopa in 10 mM pH 7.0 phosphate buffer. This solution was then mixed with a phosphate buffered solution of mushroom tyrosinase to obtain a total enzyme concentration of either 4.3 μg/mL (L-dopa substrate) or 43.3 μg/mL (tyrosine substrate) (29, 31). The solutions were maintained at 25 ^{o}C for up to five minutes while initial rate of dopachrome formation (475 nm) was monitored (32-34). There was no evidence of dopachrome production when the naphthalene imides were incubated with mushroom tyrosinase without substrate. As a control, **NI-Ala** had no effect on either the monophenolase or diphenolase activity of the enzyme. The results are shown in Figures 7 and 8.

The kinetics of dopachrome formation as a function of added **NI-Dopa** are shown in Figure 7. When tyrosine is used as a substrate to monitor the monophenolase activity, there is a lag time before the reaction reaches steady state (36-37). The lag time (time to linearity) was dependent on the concentration of **NI-Dopa.** The reaction curve for diphenolase activity shown in Figure 7b, shows the addition of **NI-Dopa** increases the rate of dopachrome formation. The same effects were seen from the addition of **NI-Tyr** to the monophenolase and diphenolase activity of mushroom tyrosinase. The data were then fitted to the Michaelis-Menten equation and shown in Figure 8.

The enzymatic conversion of L-dopa to dopachrome (diphenolase activity) was modified by the naphthalimides. Plots of the initial reaction velocity vs. L-dopa concentration, as a function of added **NI-Tyr** or **NI-Dopa**, are shown in Figures 8a and 8b, respectively. Addition of the naphthalimides increased the reaction velocity of mushroom tyrosinase. The data were fitted to the Michaelis-Menten model (eq 1) and are summarized in Table 2. The V_{max} increased as a function of added naphthalimide, while the K_m decreased.

Addition of 100 µM **NI-Dopa** and **NI-Tyr** increased V_{max} by about 20% consistent with the plots shown in Figure 8a and 8b. A decrease in K_m suggests the naphthalimides caused a stronger association of mushroom tyrosinase with L-dopa and the increase in V_{max} indicates a faster substrate turn-over rate. The addition of naphthalimides altered both kinetic parameters which indicated a mixed activation of the diphenolase activity by the naphthalimides.

In contrast, the addition of naphthalimides inhibited the monophenolase activity of mushroom tyrosinase. At the tyrosine concentrations used, the reaction velocity of the monophenolase activity was diminished by addition of either **NI-Tyr** or **NI-Dopa.** The results are shown in Figures 8c and 8d and indicate a slower conversion of tyrosine to dopachrome. The data were fitted to the Michaelis-Menten equation and the kinetic parameters are shown in Table 3. At 67 µM **NI-Dopa** and 200 µM **NI-Tyr**, the data no longer fit to the Michaelis-Menten model, but to a linear model. Slopes of these lines decreased with addition of naphthalimide. Both the V_{max} and K_m increased as a function of added naphthalimide according to the Michaelis-Menten model. Data could not be obtained to verify an increase in V_{max} at saturating conditions due to the limited solubility of tyrosine at pH 7.0. An increase in K_m suggests that **NI-Tyr** and **NI-Dopa** disrupt enzyme-substrate complex formation. The increase in K_m was larger for **NI-Dopa**. The modification of both kinetic parameters in the Michaelis-Menten model indicated a mixed inhibition of the monophenolase activity by the naphthalimides.

The results shown in Figures 6-8 suggest specific interactions between mushroom tyrosinase and the tyrosine- or dopa-substituted 1,8-naphthalimides. The increase in naphthalimide fluorescence intensity upon incubation with mushroom tyrosinase suggests

enzymatic modification of the covalently attached tyrosine or dopa. However, no dopachrome formation is observed from the NI-substrate conjugates. This allows a convenient way to monitor how enzymatic conversions of either tyrosine or L-dopa are modified by the naphthalimides. Monophenolase activity (conversion of free tyrosine to dopachrome) is inhibited. Conversely, diphenolase activity (conversion of L-dopa to dopachrome) is activated. In both cases, deviations in both kinetic parameters occur, indicating association of **NI** affects mushroom tyrosinase activity.

DISCUSSION

Photophysical deactivation pathways of the naphthalimides

The spectra shown in Figure 3 indicate that conjugation of tyrosine or dopa to 1,8-naphthalimides introduces a singlet-state (S_1) deactivation pathway that is not present in **NI-Ala**. We have previously shown that tyrosine quenches the singlet state of **NI-Ala** at diffusion-controlled rates (21). The rate constant for quenching by lysozyme is almost 2 orders of magnitude larger than that expected for a diffusion-controlled process. We attribute this to the existence of multiple quenchers on the enzyme surface. That is, each collision complex actually presents multiple quenchers to the S_1 state of **NI**. The alternative explanation of weak complex formation between the naphthalmide and enzyme cannot be ruled out, although no evidence of this was observed in the UV absorption spectrum. This quenching is attributed to photoinduced electron transfer from the phenol or the catechol to the S_1 state of **NI**. The exergonicity of this process is estimated from eq (3).

$$\Delta G_{ET} = E_{ox} - E_{1/2}(NI/NI^{\cdot-}) - E_{S1} + \Delta E_{Coulombic} \qquad (3)$$

In eq (3), E_{ox} is the oxidation potential of the phenol (or catechol): $E_{1/2}(TyrH^{\bullet+}/Tyr) = 0.94$ eV and $E_{1/2}(DopaH^{\bullet+}/Dopa) = 0.745$ vs NHE (38, 39). Using the reduction potential of the naphthalimide ($E_{1/2}(NI/NI^{\cdot-}) = -1.01$ vs NHE), along with the S_1 energy (3.35 eV), the free-energy change for photoinduced electron transfer from tyrosine and dopa the S_1 state of **NI** is estimated to be 1.4 and 1.6 eV, respectively (21). The magnitude of the solvation change upon electron transfer ($\Delta E_{Coulombic}$) is estimated to be small (0.004 eV) in aqueous solution. Therefore, the low fluorescence quantum yields of **NI-Tyr** and **NI-Dopa** are attributed to an intramolecular electron transfer from the phenol or catechol to the singlet excited-state of the naphthalene imide.

The energetics of photoinduced electron transfer from tyrosine to the S_1 state of the naphthalimide are shown in Figure 9. As described above, exergonic pathway (a) accounts for the low fluorescence quantum yields of **NI-Tyr** (and **NI-Dopa**) compared to **NI-Ala**. When the conjugates are incubated with mushroom tyrosinase, the fluorescence is restored (Figure 6). Addition of mushroom tyrosinase to a solution of **NI-Ala** did not change its fluorescence intensity. Thus, the results are consistent with enzymatic oxidation of the covalently attached tyrosine (or dopa) to ortho-quinone (Q). Dopachrome is not observed as an oxidation product (as evidenced by lack of 475-nm absorption) of **NI-Tyr** or **NI-Dopa**. The primary amine required for dopachrome formation is unavailable in the covalent conjugates. Thus, we propose that the higher oxidation potential of Q (vs. Tyr) makes the photoinduced electron transfer (process (b) in Figure 9) less exergonic and accounts for the increased fluorescence intensity. Density functional theory calculations support a higher oxidation potential for a quinone versus tyrosine or L-Dopa (40-42). The large oxidation potential of p-benzoquinone ($E_{1/2}(Q^{\bullet+}/Q) = 4.5$ eV vs NHE) makes the electron transfer thermodynamically unfavorable by 140 eV according to eq 3 (43-44). The oxidation

potential of o-benzoquinone is not known because the compound is unstable. This result clearly shows that **NI-Tyr** and **NI-Dopa** associate with mushroom tyrosinase in a conformation that allows enzymatic oxidation of the phenol or catechol portion of the conjugate. It also offers a novel "turn-on" fluorescent probe to assess enzymatic activity or screen potential inhibitors (45-46).

Non-specific crosslinking of lysozyme

We have previously reported the triplet-mediated lysozyme oxidation using **NI-Ala** and **NI-Tyr** (21). The report demonstrated that irradiation of **NI-Ala** or **NI-Tyr** in the presence of lysozyme produced dimers. The dimer yield was much lower for **NI-Tyr**, consistent with the results shown in Figure 5. In addition to the lysozyme dimers, the results shown in Figure 5 indicate formation of trimers. The Figure also shows that the crosslinking yield of **NI-Dopa** is equivalent to that of **NI-Tyr**. Based on previous work, we propose that formation of the crosslinked photoproducts is initiated by electron transfer from a surface-accessible amino acid to the triplet excited-state of the naphthalimide. The low fluorescence quantum yields of **NI-Tyr** and **NI-Dopa** suggest a very rapid electron transfer from the covalently attached phenol or catechol to the S_1 state of **NI**. This is supported by the energy level diagram shown in Figure 9. Since this process is in competition with intersystem crossing to form the **NI** triplet state (^{3}**NI***), the yield of ^{3}**NI*** in both **NI-Tyr** and **NI-Dopa** is very low. Thus, we propose that oxidative crosslinking of lysozyme by **NI-Ala**, **NI-Tyr** and **NI-Dopa** is predominantly mediated by a triplet excited state that is produced in low yield when singlet-mediated intramolecular electron transfer (from tyr or dopa) occurs. Lysozyme contains 3 tyrosine, 6 tryptophan and 1 histidine, 2 methionine and 8 cysteine (47). These amino acids

have oxidizable side chains that are potential sites for oxidative crosslinking. While the results shown in Figure 5 clearly indicate that the naphthalimide excited states oxidatively modify the protein, the site (or sites) of modification is unclear.

Modification of mushroom tyrosinase activity

Competitive enzyme kinetics with the naphthalimide conjugates were performed to verify the site of interaction within mushroom tyrosinase. As shown in Figure 8, the diphenolase activity was activated and the monophenolase activity of mushroom tyrosinase was inhibited in the presence of the naphthalimides. **NI-Tyr** and **NI-Dopa** did not cyclize or polymerize to products that absorbed at 475 nm during the 2-5 minute enzyme experiment. Thus, dopachrome formation occurs only from the native tyrosine or L-dopa substrates (48). For both activities, the K_m and V_{max} values changed as a function of naphthalimide concentration. Therefore, the mechanism of activation, as well as inhibition, was attributed to a mixed activation/inhibition type. Collectively, the results suggest that the naphthalimides interact with multiple sites of mushroom tyrosinase.

Mixed activation of diphenolase activity and inhibition of the monophenolase activity has been reported with the glycosylated phenol, α-arbutin. The kinetic data were directly comparable to our naphthalimide results (33). The increase in monophenolase lag time with added α-arbutin, as well as alteration of both V_{max} and K_m, is similar to the results shown in Figure 7a and summarized in Table 3 (33). Likewise, enhancement in diphenolase activity and modification of both V_{max} and K_m (Table 2) were observed with α-arbutin. It was proposed that the addition of α-arbutin activated the diphenolase activity by interacting with

residues located at the entrance to the active site and decreased the effect of suicide inactivation (33). That study suggested the conformation change was induced by hydrophobic interactions between the histidine and methionines in the entrance to the active site, making the binding to L-dopa more favorable and inhibiting tyrosine oxidation (33). Current literature also suggests that the activation of mushroom tyrosinase by detergents, metal ions, oligopeptides and catechol-based (substrate) compounds is due to binding of copper ions within the active site that alter the structure and mechanism of oxidation (49-52). Due to the similarities in enzyme kinetics between the naphthalimides and α-arbutin, we conclude that the phenol group of the naphthalimides interacts with the active site and modifies the residues. This modification decreases both the suicide inactivation and monophenolase activity, but increases the diphenolase kinetics.

The fluorescence assay in Figure 6 suggests these naphthalimide are substrates for mushroom tyrosinase. The competitive kinetic experiments were repeated with a known substrate, N-acetyl-tyrosine to understand how the compound would alter the diphenolase and monophenolase activity of mushroom tyrosinase (53). Mushroom tyrosinase catalyzes the oxidation of N-acetyl-tyrosine to N-acetyl dopaquinone. However the product cannot cyclize to form the dopachrome product that is observed in the 475-nm absorption assay (53). The addition of N-acetyl-tyrosine inhibited monophenolase activity and activated the diphenolase activity of mushroom tyrosinase (Supporting Information, Figure S1). The similarity in the kinetic data between the known substrates, N-acetyl-tyrosine, α-arbutin, and the naphthalimide conjugates supports the hypothesis that **NI-Tyr** and **NI-Dopa** interact with the active site of mushroom tyrosinase.

Oxidation of both tyrosine and L-dopa occur in the same active site of mushroom tyrosinase (36-37). The enzyme has four oxidation states, as determined by circular dichroism: oxy-, deoxy-, met- and deact-tyrosinase. Each of these states plays a different role

in the enzyme's oxidative catalysis. The states are interconverted during catalysis, as shown in Scheme 1 (36-37,48). The reductive elimination of copper in the deact-tyrosinase is irreversible and permanently deactivates the enzymes (54). Oxy-tyrosinase state is the only form of the enzyme that has been confirmed by crystal structure (55-57). Tyrosine oxidation can only occur from the oxy-tyrosinase state, while L-dopa can be converted to dopaquinone by both the oxy- and met-tyrosinase states (36-37). The orientation of L-dopa in the hydrophobic active site of oxy- tyrosinase is sterically favored over tyrosine, accounting for the enzyme's higher specific activity for L-dopa (36).

The lag time associated with monophenolase activity is observed with all monophenol substrates (36-37). Initial tyrosine oxidation is slow and then accelerates to reach steady state after this lag period. The lag period is associated with conversion of met-tyrosinase to oxy-tyrosinase, via the deoxy-tyrosinase intermediate. The majority of native mushroom tyrosinase is in the met-form (36),(48). A small amount of oxy-tyrosinase is present in native mushroom tyrosinase. This form oxidizes tyrosine to dopaquinone, which can further cyclize to leucodopachrome. Redox exchange between dopaquinone and leucodopachrome forms L-dopa and dopachrome (36). Thus, small amounts of the monophenolase activity indirectly generate L-dopa from tyrosine. L-dopa can react with met-tyrosinase to form deoxy-tyrosinase, which then rapidly reacts with oxygen to form oxy-tyrosinase and catalyzes the oxidation of tyrosine.

Based on current literature, we propose the naphthalimides interact with the active site of mushroom tyrosinase by shifting the equilibrium between oxidation states within the active site, as shown in Scheme 1 (33,36,50-51). An increase in V_{max} for both the monophenolase and diphenolase activity is attributed to a decreased effect of suicide inactivation from oxy-

tyrosinase to deact-tyrosinase (33). Less of the enzyme was deactivated with **NI-Tyr** and **NI-Dopa**, which increased the concentration of available enzyme. Because V_{max} is a function of total enzyme concentration, this parameter increased.

The naphthalimides induced opposite effects on K_m in the monophenolase and diphenolase catalysis by shifting the equilibrium away from oxy-tyrosinase, to met-tyrosinase. This shift may be concomitant with modification of amino acids in the active site. The binding affinity was increased during diphenolase because the enzyme was in the correct orientation for L-dopa to bind in the met-tyrosinase active site (33). The addition of **NI-Tyr** and **NI-Dopa** increased the lag time in the monophenolase catalysis, indicating that the enzyme took longer to convert to the oxy-tyrosinase state (33). Oxy-tyrosinase is the only oxidation state of mushroom tyrosinase that can convert tyrosine to a quinone. We propose that the naphthalimide conjugates enhanced the conversion of oxy- to met-tyrosinase, thus decreasing the observed rate of tyrosine oxidation. The increased in tyrosine K_m is thought to be due to a conformational change induced by the naphthalimide conjugates. It is proposed that phenols (tyrosine) and catechols (dopa) associate with different copper ions in the active site of tyrosinase (54). The higher specific activity for catechols is attributed to the orientation (with respect to copper) of the substrate within the enzyme active site. Thus, conversion of the oxy- to met-tyrosinase, induced by the naphthalimide conjugates, favors a form that binds monophenols much more weakly than catechols. Thus, we suggest that the lower affinity of tyrosine upon addition of the naphthalimide conjugates results from the shift in equilibrium from the oxy- to met-forms of the enzyme. The data that did not fit to the Michaelis-Menten model, but to a linear model, showed a decrease in slope upon the addition of naphthalimides. These data indicate that, at the tyrosine concentrations used, the enzyme never reached saturating-substrate concentrations. Lack of curvature in the data indicates a low affinity for tyrosine and an increased K_m which may be attributed to a conformation

change in the active site of mushroom tyrosinase. Conformational and oxidation changes of mushroom tyrosinase were not assessed in this study.

Photomodification of mushroom tyrosinase activity

The naphthalimide conjugates crosslinked lysozyme with no evidence of site-specificity. However, only the **NI-Tyr** and **NI-Dopa** conjugates (not **NI-Ala**) affected the enzymatic activity of mushroom tyrosinase, suggesting site-specific interactions. Thus, the naphthalimides were irradiated in the presence of mushroom tyrosinase to assess the photoinduced modification of enzyme activity. Solutions (2.50 mL) of 100 μM **NI-Tyr**, **NI-Dopa** or **NI-Ala** and 4.33 μg/mL mushroom tyrosinase in pH 7.0 phosphate buffer were irradiated in a turn table reactor at 25 ^{o}C for 1 hour. Control solutions were simultaneously prepared and incubated in the dark for the same time duration. 0.50 mL of a 6 mM L-dopa was then added to each solution after incubation/irradiation and dopachrome formation was monitored at 475 nm for 2 minutes (as shown in Figure 7b). The diphenolase activity was determined from the slope of A(475 nm) vs. time plot. Mushroom tyrosinase, irradiated as a control in the absence of **NI**, retained 95 % of its diphenolase activity, compared to the dark control. The rate of dopachrome formation was unchanged in the dark control containing **NI-Ala**, suggesting no non-specific enzyme modification. However, the diphenolase activity dropped after dark incubation with **NI-Tyr** and **NI-Dopa** to 83% and 79% respectively. The fluorescence increase shown in Figure 6 is attributed to (dark) enzymatic conversion of the phenol or catechol to a quinone. Thus, we attribute the loss of diphenolase activity upon dark incubation with NI-Tyr or NI-DOPA to build-up of polymerized NI-quinone overoxidation products that inhibit the enzyme. Significantly, when the **NI** compounds were irradiated in

the presence of mushroom tyrosinase, the decrease in diphenolase activity was larger than that observed in the dark control. The enzyme activity was decreased by 53% and 48%, respectively, in irradiated solutions of **NI-Tyr** and **NI-Dopa**, respectively. A smaller decrease (to 84%) in diphenolase activity was observed in the solution of irradiated **NI-Ala**. We tentatively attribute the results to crosslink formation within or near the mushroom tyrosinase active site, formed only when the **NI** is conjugated with the tyr or dopa substrate analog. This crosslinking would inhibit the dopa substrate from entering the enzyme active site. Thus, while dark incubation inhibited diphenolase activity due to the formation of enzymatic oxidation products (quinones), photoinduced modification of the enzyme itself had a significantly larger effect on its activity. The effect was higher when a naphthalimide-substrate conjugate (**NI-Tyr** or **NI-DOPA**) was used, suggesting that the site of modification was specific to the enzyme's active site.

CONCLUSIONS

This study demonstrates the potential of **NI-Ala** as a photooxidative crosslinker to probe protein complex formation. Phenol-functionalized naphthalimides had low triplet-mediated protein crosslinking yields due to an intramolecular photoinduced electron transfer. **NI-Tyr** and **NI-Dopa** were utilized as a fluorescent turn-on probes when oxidized within the active site of mushroom tyrosinase. The enzymatic oxidation modified the thermodynamics of photoinduced electron transfer and increased the fluorescence of the naphthalimides. Active-site specificity was verified by competitive enzyme kinetics which showed modification of the catalytic activity by the naphthalimide conjugates. Further modification of these conjugates offers the prospect of generating biologically relevant active site modification or crosslinking, coupled with a light-up fluorescent probe of active-site binding.

SUPPORTING INFORMATION

Additional supporting information may be found online in the Supporting Information section at the end of the article:

Figure S1. Kinetic curves for the (a) diphenolase activity of 0.5 μg/mL mushroom tyrosinase and (b) monophenolase activity of 5.0 μg/mL mushroom tyrosinase in 10mM phosphate buffer pH 7.0 with increasing concentrations of N-acetyl-tyrosine (**NAT**). 0 mM (circle) 0.1 mM (square) 0.2 mM (triangle) 0.3 mM N-acetyl-tyrosine (diamond).

ACKNOWLEDGEMENT. This work was supported by the Department of Chemistry and Biochemistry, University of Maryland, Baltimore County.

REFERENCES.

1. Amini, F., C. Denison, H. J. Lin, L. Kuo and T. Kodadek (2003) Using oxidative crosslinking and proximity labeling to quantitatively characterize protein-protein and protein-peptide complexes. *Chem. Biol.* **10,** 1115-1127.

2. Scientific, T. F. (2009) Thermo Scientific Pierce Crosslinking Technical Handbook. Available at: http://tools.thermofisher.com/content/sfs/brochures/1602163-Crosslinking-Reagents-Handbook.pdf.

3. Fields, S. and O. K. Song (1989) A novel genetic system to detect protein-protein interactions. *Nature (London)* **340,** 245-246.

4. Waugh, D. F. (1954) Protein-Protein Interactions. In *Advances in Protein Chemistry*, Vol. 9. (Edited by M. L. Anson, K. Bailey and J. T. Edsall), pp. 325-437. Academic Press.

5. Fancy, D. A. and T. Kodadek (1999) Chemistry for the Analysis of Protein-Protein Interactions: Rapid and Efficient Cross-Linking Triggered by Long Wavelength Light. *Proc. Natl. Acad. Sci. USA* **96,** 6020-6024.

6. Fancy, D. A. and T. Kodadek (1997) Site-Directed Oxidative Protein Cross-linking. *Tetrahedron* **53,** 11953-11960.

7. Preston, G. (2013) Photo-induced covalent cross-linking for the analysis of biomolecular interactions. *Chem. Soc. Rev.* **42,** 3289-3301.

8. Borsarelli, C. D., L. J. Falomir-Lockhart, V. Ostatna, J. A. Fauerbach, H. H. Hsiao, H. Urlaub, E. Palecek, E. A. Jares-Erijman and T. M. Jovin (2012) Biophysical properties and cellular toxicity of covalent crosslinked oligomers of alpha-synuclein formed by photoinduced side-chain tyrosyl radicals. *Free Radical Biol. Med.* **53,** 1004-1015.

9. Preston, G. W., S. E. Radford, A. E. Ashcroft and A. J. Wilson (2012) Covalent Cross-Linking within Supramolecular Peptide Structures. *Anal. Chem.* **84,** 6790-6797.

10. Bitan, G. and D. B. Teplow (2004) Rapid Photochemical Cross-LinkingA New Tool for Studies of Metastable, Amyloidogenic Protein Assemblies. *Acc. Chem. Res.* **37,** 357-364.

11. Maji, S. K., R. R. Ogorzalek Loo, M. Inayathullah, S. M. Spring, S. S. Vollers, M. M. Condron, G. Bitan, J. A. Loo and D. B. Teplow (2009) Amino Acid Position-specific Contributions to Amyloid β-Protein Oligomerization. *J. Biol. Chem.* **284,** 23580-23591.

12. Roychaudhuri, R., A. Lomakin, S. Bernstein, X. Y. Zheng, M. M. Condron, G. B. Benedek, M. Bowers and D. B. Teplow (2014) Gly25-Ser26 Amyloid a-Protein Structural lsomorphs Produce Distinct A beta 42 Conformational Dynamics and Assembly Characteristics. *J. Mol. Biol.* **426,** 2422-2441.

13. Alarcon, E. I., H. Poblete, H. Roh, J.-F. Couture, J. Comer and I. E. Kochevar (2017) Rose Bengal Binding to Collagen and Tissue Photobonding. *ACS Omega* **2,** 6646-6657.

14. Elvin, C. and T. Vuocolo (2011) Photochemical Crosslinking of Proteins to Make Novel Biomedical Materials. *Aust. Biochem.* **42,** 15-18.

15. Yao, M., A. Yaroslavsky, F. P. Henry, R. W. Redmond and I. E. Kochevar (2010) Phototoxicity is not associated with photochemical tissue bonding of skin. *Lasers in Surgery and Medicine* **42,** 123-131.

16. Cherfan, D., E. E. Verter, S. Melki, T. E. Gisel, F. J. Doyle, G. Scarcelli, S. H. Yun, R. W. Redmond and I. E. Kochevar (2013) Collagen Cross-Linking Using Rose Bengal and Green

Light to Increase Corneal Stiffness. *Investigative Ophthalmology & Visual Science* **54,** 3426-3433.

17. Roberts, C. J., W. J. Dupps and J. C. Downs (2018) *Biomechanics of the Eye.* Kruger Publication, Amsterdam.

18. Kodadek, T., I. Duroux-Richard and J. C. Bonnafous (2005) Techniques: Oxidative cross-linking as an emergent tool for the analysis of receptor-mediated signalling events. *Trends Pharmacol. Sci.* **26,** 210-217.

19. Tomczyk, M. D. and K. Z. Walczak (2018) 1,8-Naphthalimide based DNA intercalators and anticancer agents. A systematic review from 2007 to 2017. *Eur. J. Med. Chem.* **159,** 393-422.

20. Banerjee, S., E. B. Veale, C. M. Phelan, S. A. Murphy, G. M. Tocci, L. J. Gillespie, D. O. Frimannsson, J. M. Kelly and T. Gunnlaugsson (2013) Recent advances in the development of 1,8-naphthalimide based DNA targeting binders, anticancer and fluorescent cellular imaging agents. *Chem. Soc. Rev.* **42,** 1601-1618.

21. Abraham, B. and L. A. Kelly (2003) Photooxidation of amino acids and proteins mediated by novel 1,8-naphthalimide derivatives. *J. Phys. Chem. B* **107,** 12534-12541.

22. Rogers, J. E., S. J. Weiss and L. A. Kelly (2000) Photoprocesses of naphthalene imide and diimide derivatives in aqueous solutions of DNA. *J. Am. Chem. Soc.* **122,** 427-436.

23. Woods, R. J., J. X. Zhang, C. R. Green and R. R. Kane (2003) Protein crosslinking by 1,8-naphthalimides: influence of the 4-substituent. *Arkivoc***,** 109-118.

24. Zhang, J. X., R. J. Woods, P. B. Brown, R. A. Mowery, R. R. Kane, R. W. Jackson and F. Pollo (2004) Photochemical tissue bonding using monomeric 4-amino-1,8-naphthalimides. *J. Biomed. Optics* **9,** 1089-1092.

25. Munger, K. A., T. M. Downey, B. Haberer, K. Pohlson, L. L. Marshall and R. E. Utecht (2016) A novel photochemical cross-linking technology to improve luminal gain, vessel compliance, and buckling post-angioplasty in porcine arteries. *J. Biomed. Mater. Res., Part B* **104,** 375-384.

26. Pace, C. N., F. Vajdos, L. Fee, G. Grimsley and T. Gray (1995) How to measure and predict the molar absorption coefficient of a protein. *Protein Sci.* **4,** 2411-2423.

27. Seo, S. Y., V. K. Sharma and N. Sharma (2003) Mushroom tyrosinase: Recent prospects. *J. Agric. Food Chem.* **51,** 2837-2853.

28. Rogers, J. E., B. Abraham, A. Rostkowski and L. A. Kelly (2001) Mechanisms of photoinitiated cleavage of DNA by 1,8-naphthalimide derivatives. *Photochem. Photobiol.* **74,** 521-531.

29. Abu Ubeid, A. and B. M. Hantash (2014) Novel Pentapeptide Activators of Mammalian and Mushroom Tyrosinase. *Curr. Top. Med. Chem.* **14,** 1463-1468.

30. Saghaie, L., M. Pourfarzam, A. Fassihi and B. Sartippour (2013) Synthesis and tyrosinase inhibitory properties of some novel derivatives of kojic acid. *Res. Pharm. Sci.* **8,** 233-242.

31. Qiu, L., J.-x. Zhuang, F.-j. Liu, M.-h. Yang, J.-j. Zhou, Z.-c. Li and Q.-x. Chen (2009) Inhibitory effects of 4-aminobenzoic acid on mushroom tyrosinase. *Xiamen Daxue Xuebao, Ziran Kexueban* **48,** 302-304.

32. Amin, E., A. A. Saboury, H. Mansuri-Torshizi and A. A. Moosavi-Movahedi (2010) Potent inhibitory effects of benzyl and p-xylidine-bis dithiocarbamate sodium salts on activities of mushroom tyrosinase. *Journal of Enzyme Inhibition and Medicinal Chemistry* **25,** 272-281.

33. Qin, L., Y. Wu, Y. T. Liu, Y. M. Chen and P. Zhang (2014) Dual Effects of Alpha-Arbutin on Monophenolase and Diphenolase Activities of Mushroom Tyrosinase. *Plos One* **9,** 7.

34. Chen, L. H., Y. H. Hu, W. Song, K. K. Song, X. Liu, Y. L. Jia, J. X. Zhuang and Q. X. Chen (2012) Synthesis and Antityrosinase Mechanism of Benzaldehyde Thiosemicarbazones: Novel Tyrosinase Inhibitors. *J. Agric. Food Chem.* **60,** 1542-1547.

35. Turro, N. J., V. Ramamurthy and J. C. Scaiano (2009) *Principles of Molecular Photochemistry : An Introduction.* University Science Books, Sausalito, Calif.

36. Ramsden, C. A. and P. A. Riley (2014) Tyrosinase: The four oxidation states of the active site and their relevance to enzymatic activation, oxidation and inactivation. *Bioorg. Med. Chem.* **22,** 2388-2395.

37. Deri, B., M. Kanteev, M. Goldfeder, D. Lecina, V. Guallar, N. Adir and A. Fishman (2016) The unravelling of the complex pattern of tyrosinase inhibition. *Scientific Reports* **6,** 10.

38. Eslami, M., H. R. Zare and M. Namazian (2012) Thermodynamic Parameters of Electrochemical Oxidation of L-DOPA: Experimental and Theoretical Studies. *J. Phys. Chem. B* **116,** 12552-12557.

39. DeFelippis, M. R., C. P. Murthy, F. Broitman, D. Weinraub, M. Faraggi and M. H. Klapper (1991) Electrochemical properties of tyrosine phenoxy and tryptophan indolyl radicals in peptides and amino acid analogues. *J. Phys. Chem.* **95,** 3416 - 3419.

40. Huq, F. (2007) Molecular Modelling Analysis of the Metabolism of Naphthalene. *J. Pharmacol. Tox.* **2007,** 33-43.

41. Ledwon, P., A. Brzeczek, S. Pluczyk, T. Jarosz, W. Kuznik, K. Walczak and M. Lapkowski (2014) Synthesis and electrochemical properties of novel, donor-acceptor pyrrole derivatives with 1,8-naphthalimide units and their polymers. *Electrochim. Acta* **128,** 420-429.

42. Makuraza, J., T. Pogrebnaya and A. Pogrebnoi (2015) Vibrational and Electronic Spectra of Natural Dyes Constituents for Solar Cell Application: DFT and TDDFT Study. *Int. J. Mat. Sci. App.* **4,** 314-324.

43. Raymond, K. S., A. K. Grafton and R. A. Wheeler (1997) Calculated one-electron reduction potentials and solvation structures for selected p-benzoquinones in water. *J. Phys. Chem. B* **101,** 623-631.

44. Huang, J. H., B. F. Pan, W. T. Duan, X. L. Wei, R. S. Assary, L. Su, F. R. Brushett, L. Cheng, C. Liao, M. S. Ferrandon, W. Wang, Z. C. Zhang, A. K. Burrell, L. A. Curtiss, I. A. Shkrob, J. S. Moore and L. Zhang (2016) The lightest organic radical cation for charge storage in redox flow batteries. *Scientific Reports* **6,** 9.

45. Kim, T.-I., J. Park, S. Park, Y. Choi and Y. Kim (2011) Visualization of tyrosinase activity in melanoma cells by a BODIPY-based fluorescent probe. *Chem. Commun.* **47,** 12640-12642.

46. Sunahara, H., Y. Urano, H. Kojima and T. Nagano (2007) Design and synthesis of a library of BODIPY-based environmental polarity sensors utilizing photoinduced electron-transfer-controlled fluorescence ON/OFF switching. *J. Am. Chem. Soc.* **129,** 5597-5604.

47. Canfield, R. (1963) The amino acid sequence of egg white lysozyme. *J. Biol. Chem.* **238,** 2698-2707.

48. Chang, T. S. (2009) An Updated Review of Tyrosinase Inhibitors. *Int. J. Mol. Sci.* **10,** 2440-2475.

49. Gheibi, N., A. Saboury and M. Sarreshtehdari (2011) Non-essential activation of Co and Zn on mushroom tyrosinase: Kinetic and structural stability. *Bull. Korean Chem. Soc.* **32,** 150-156.

50. Espín, J. C. and H. J. Wichers (1999) Activation of a Latent Mushroom (Agaricus bisporus) Tyrosinase Isoform by Sodium Dodecyl Sulfate (SDS). Kinetic Properties of the SDS-Activated Isoform. *J. Agric. Food Chem.* **47,** 3518-3525.

51. Espín, J. C. and H. J. Wichers (1999) Kinetics of Activation of Latent Mushroom (Agaricus bisporus) Tyrosinase by Benzyl Alcohol. *J. Agric. Food Chem.* **47,** 3503-3508.

52. Sanjust, E., G. Cecchini, F. Sollai, N. Curreli and A. Rescigno (2003) 3-hydroxykynurenine as a substrate/activator for mushroom tyrosinase. *Arch. Biochem. Biophys.* **412,** 272-278.

53. Kahn, V. and N. Ben-Shalom (1998) N-acetyl-L-tyrosine as a substrate for mushroom tyrosinase. *Pigment Cell Res.* **11,** 24-33.

54. Ramsden, C. A. and P. A. Riley (2010) Mechanistic studies of tyrosinase suicide inactivation. *Arkivoc***,** 260-274.

55. Matoba, Y., T. Kumagai, A. Yamamoto, H. Yoshitsu and M. Sugiyama (2006) Crystallographic evidence that the dinuclear copper center of tyrosinase is flexible during catalysis. *J. Biol. Chem.* **281,** 8981-8990.

56. Mauracher, S. G., C. Molitor, R. Al-Oweini, U. Kortz and A. Rompel (2014) Latent and active abPPO4 mushroom tyrosinase cocrystallized with hexatungstotellurate(VI) in a single crystal. *Acta Crystallogr. Sect. D* **70,** 2301-2315.

57. Ismaya, W. T., H. J. Rozeboom, A. Weijn, J. J. Mes, F. Fusetti, H. J. Wichers and B. W. Dijkstra (2011) Crystal Structure of Agaricus bisporus Mushroom Tyrosinase: Identity of the Tetramer Subunits and Interaction with Tropolone. *Biochemistry* **50,** 5477-5486.

FIGURE CAPTIONS

Figure 1. Structures of amino-acid functionalized naphthalene imides (conjugates).

Figure 2. UV absorption spectrum of 50 μM naphthalene imides in 10 mM pH 7.0 phosphate buffer.

Figure 3. Fluorescence emission spectra of **NI-Ala** (solid line), **NI-Tyr** (dotted line) and **NI-Dopa** (dashed line) measured in 10 mM pH 7.0 phosphate buffer. Inset: Magnification of **NI-Tyr** and **NI-Dopa** spectra. λ_{ex} = 340 nm.

Figure 4. Fluorescence spectra of 10 μM **NI-Ala** in 10 mM pH 7.0 phosphate buffer with 0, 1, 2, 4, 6, 8 and 16 mM L-dopa. Inset: Stern-Volmer bimolecular quenching plot. λ_{ex}= 344 nm.

Figure 5. SDS-PAGE gel (stained with Coomassie Blue) of irradiated samples of 80 μM **NDI-Ala**, **NDI-Tyr** and **NDI-Dopa** in the presence of 50 μM lysozyme in 10 mM pH 7.0 phosphate buffer. Lane 1 MW markers; Lane 2 lysozyme; Lanes 3 and 6 **NI-Ala**; Lanes 4 and 7 **NI-Tyr**; Lanes 5 and 8 **NI-Dopa**.

Figure 6. Fluorescence increase of (a) **NI-Dopa** (11 μMS) and (b) **NI-Tyr** (11 μM) upon incubation with 43.3 μg/mL mushroom tyrosinase in 10 mM pH 7.0 phosphate buffer. Spectra were recorded immediately after incubation and every 30 minutes for 2 hours. λ_{ex} = 344 nm.

Figure 7. Absorbance of dopachrome at 475 nm as a function of time. (a) Solution of 43.3 μg/mL mushroom tyrosinase and 0.5 mM tyrosine with 0, 20 and 67 μM **NI-Dopa** in 10 mM pH 7.0 phosphate buffer. (b) Solution of 4.33 μg/mL mushroom tyrosinase and 0.5 mM L-Dopa with 0, 50 and 200 μM **NI-Dopa** in 10 mM pH 7.0 phosphate buffer.

Figure 8. Michaelis-Menten plots of the (a) diphenolase activity of mushroom tyrosinase with 0, 50, 100 and 200 μM **NI-Dopa** (b) diphenolase activity with 0, 50, 100 and 200 μM **NI-Tyr** (c) monophenolase activity of mushroom tyrosinase with 0, 20 and 67 μM **NI-Dopa** (d) monophenolase activity of mushroom tyrosinase with 0, 50, 100 and 200 μM **NI-Tyr** in

10 mM pH 7.0 phosphate buffer. Enzyme concentrations were 4.33 μg/mL and 43.3 μg/mL for diphenolase and monophenolase, respectively.

Figure 9. (a) Photoinduced electron transfer from tyrosine to ^{1}**NI***. (b) The process becomes thermodynamically unfavorable after conversion of the tyrosine to the o-quinone (**NI-Q**) by mushroom tyrosinase.

SCHEME CAPTION

Scheme 1. Four oxidation states of mushroom tyrosinase (oxy-, met-, deoxy- and deact-). Addition of **NI-Tyr** or **NI-Dopa** modify the distribution of the active states of the enzyme.

TABLES.

Table 1. Bimolecular quenching constant of ^{1}**NI-Ala*** by amino acids and lysozyme.

Quencher	k_q **(x 10^{9} M^{-1} s^{-1})**
Tyrosine	5.6 ± 0.6
L-dopa	3.8 ± 0.5
Lysozyme	310 ± 10

Rate constants determined using 10 μM **NI-Ala** in 10 mM pH 7.0 phosphate buffer.

Table 2. Kinetic parameters for the diphenolase activity of mushroom tyrosinase with naphthalimides.

NI-Dopa (μM)	V_{max} (μM/s)	K_m (mM)
0	1.83 ± 0.11	0.248 ± 0.015
50	1.90 ± 0.11	0.189 ± 0.011
100	1.97 ± 0.12	0.174 ± 0.010
200	2.01 ± 0.12	0.173 ± 0.010
NI-Tyr (μM)		
0	1.72 ± 0.10	0.217 ± 0.013
50	1.95 ± 0.12	0.221 ± 0.013
100	2.00 ± 0.12	0.213 ± 0.13
200	2.05 ± 0.13	0.209 ± 0.013

Solutions contained 4.33 μg/mL mushroom tyrosinase in 10 mM pH 7.0 phosphate buffer. Parameters obtained from fit to eq 1.

Table 3. Kinetic parameters for the monophenolase activity of mushroom tyrosinase with naphthalimides.

NI-Dopa (μM)	V_{max} (nM/s)	K_m (mM)
0	932 ± 83	0.167 ± 0.048
20	1269 ± 110	0.483 ± 0.043
67	---	---
NI-Tyr (μM)		
0	910 ± 82	0.154 ± 0.014
50	1193 ± 100	0.332 ± 0.030
100	3627 ± 320	2.343 ± 0.211
200	---	---

Solutions contained 43.3 μg/mL mushroom tyrosinase in 10 mM pH 7.0 phosphate buffer. Parameters obtained from fit to eq 1.

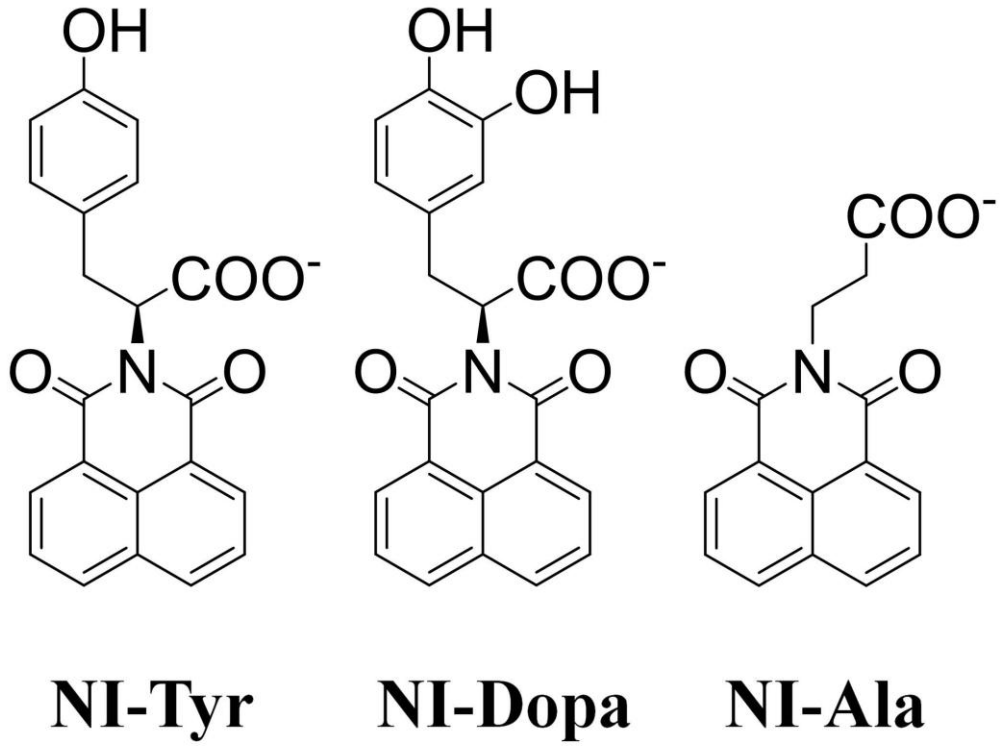

Figure 1.

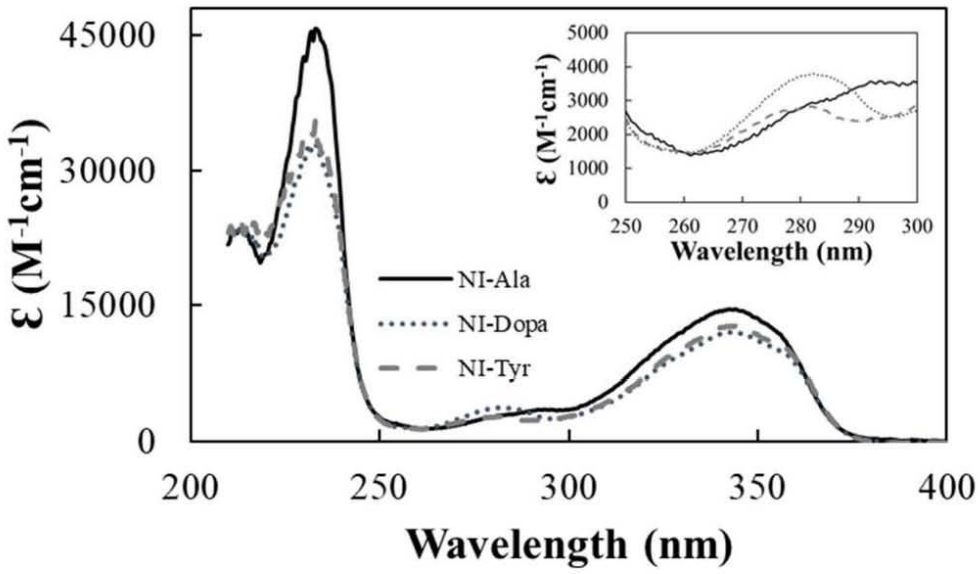

Figure 2.

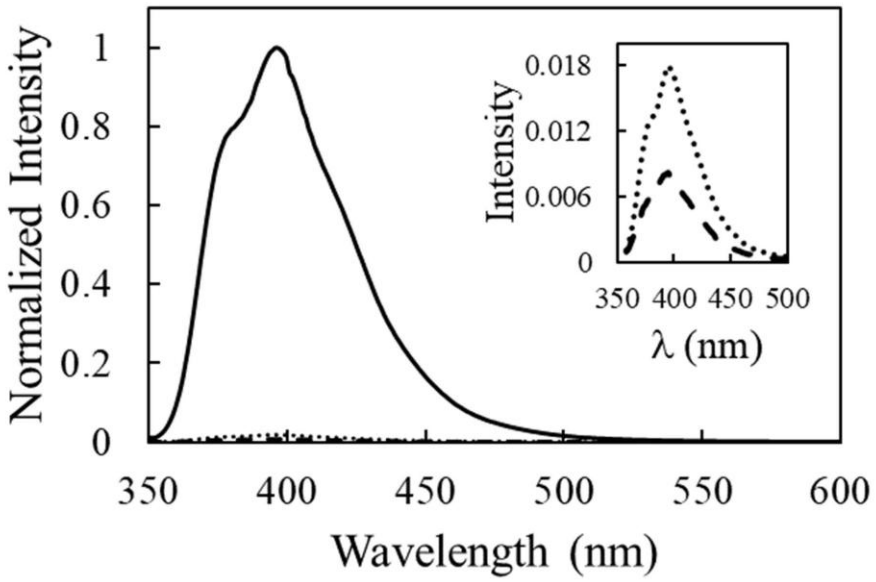

Figure 3.

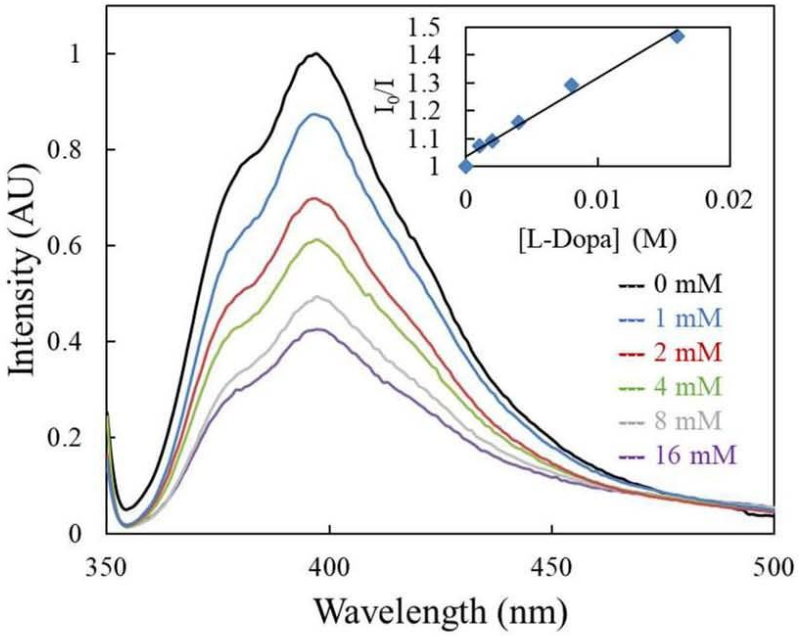

Figure 4.

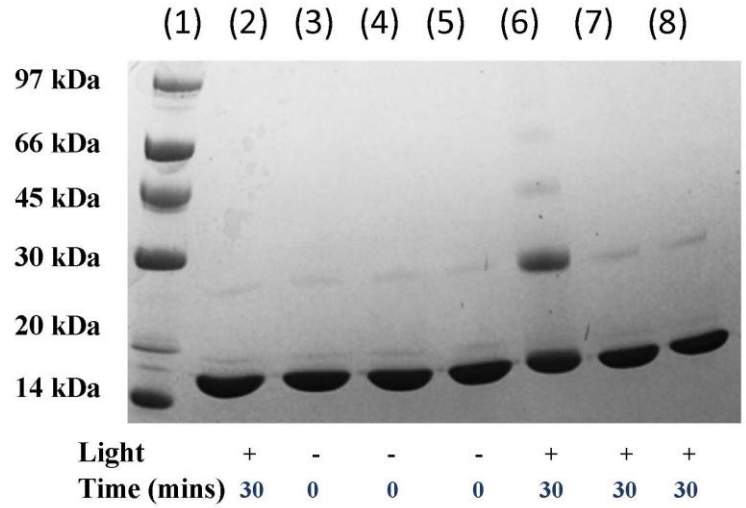

Figure 5.

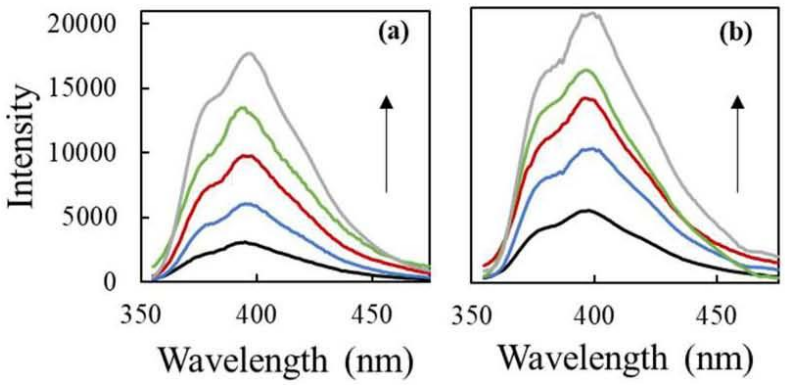

Figure 6.

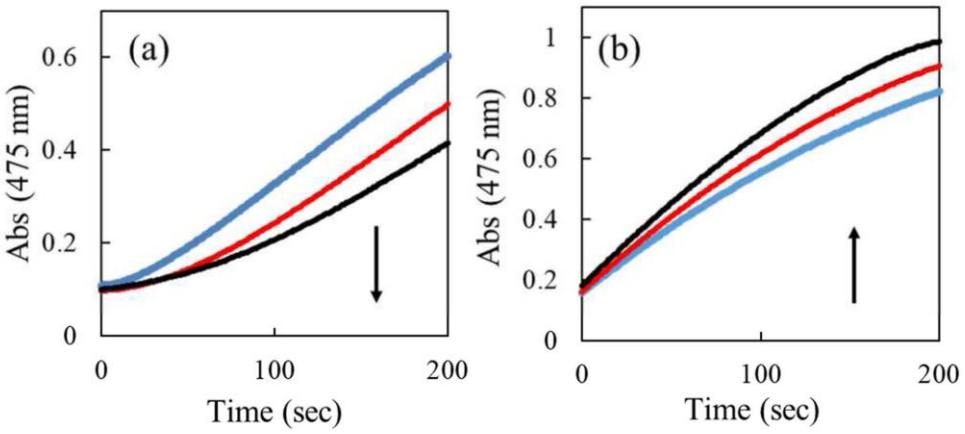

Figure 7.

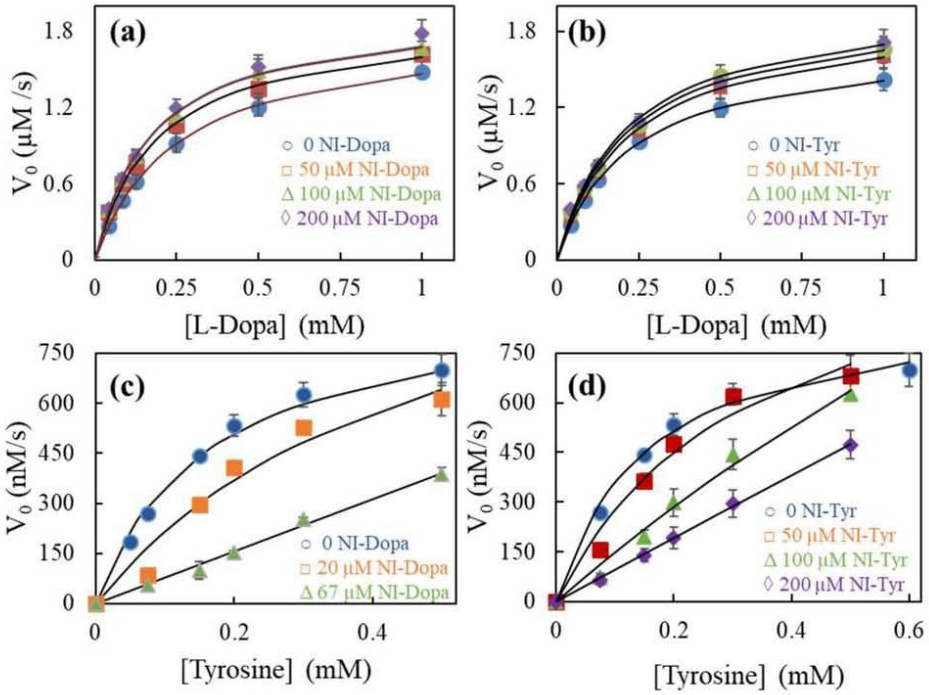

Figure 8.

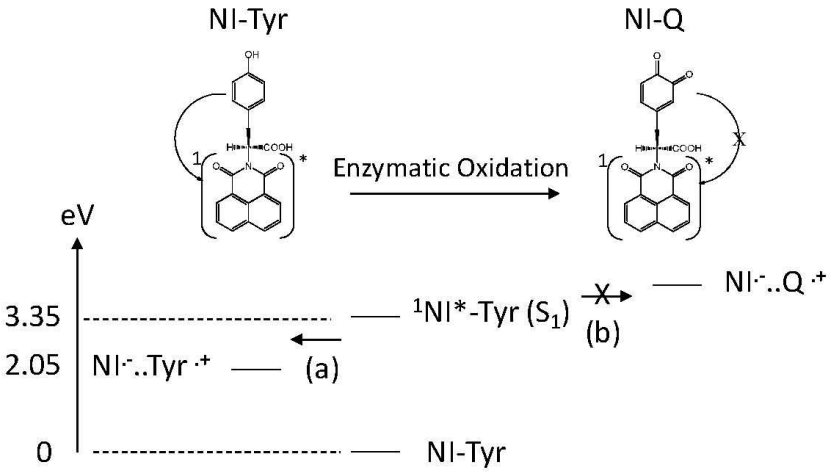

Figure 9.

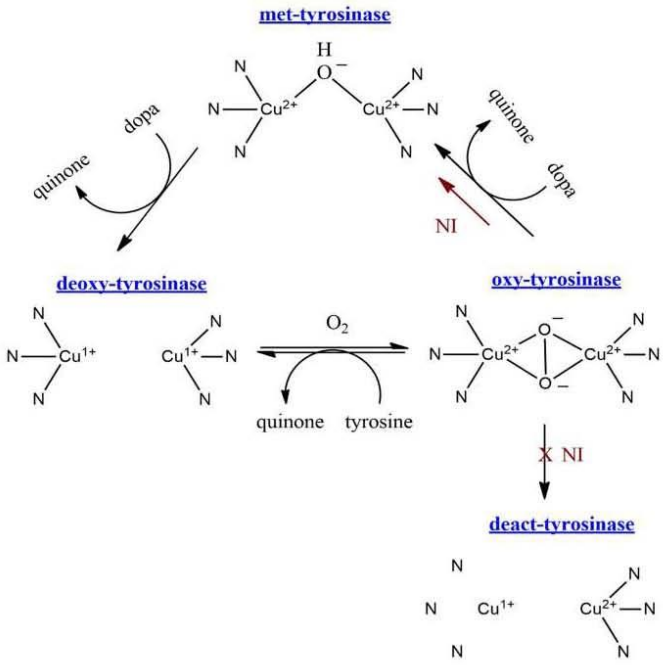

Scheme 1.